J|A|C|S ARTICLES

Published on Web 06/24/2010

Nature of the Energy Landscape for Gated Electron Transfer in a Dynamic Redox Protein

Sam Hay, Sibylle Brenner,‡ Basile Khara, Anne Marie Quinn, Stephen E. J. Rigby, and Nigel S. Scrutton*

Manchester Interdisciplinary Biocentre and Faculty of Life Science, University of Manchester, Manchester, U.K.

Received February 25, 2010; E-mail: nigel.scrutton@manchester.ac.uk

Abstract: Conformational control limits most electron transfer (ET) reactions in biology, but we lack general insight into the extent of conformational space explored, and specifically the properties of the associated energy landscape. Here we unite electron−electron double resonance (ELDOR) studies of the diradical (disemiquinoid) form of human cytochrome P450 reductase (CPR), a nicotinamide adenine phosphate dinucleotide (NADPH)-linked diflavin oxidoreductase required for P450 enzyme reduction, with functional studies of internal ET to gain new insight into the extent and properties of the energy landscape for conformationally controlled ET. We have identified multiple conformations of disemiquinoid CPR, which point to a rugged energy landscape for conformational sampling consistent with functional analysis of ET using high-pressure stopped-flow, solvent, and temperature perturbation studies. Crystal structures of CPR have identified discrete "closed" and "open" states, but we emphasize the importance of a continuum of conformational states across the energy landscape. Within the landscape more closed states that favor internal ET are formed by nucleotide binding. Open states that enable P450 enzymes to gain access to electrons located in the FMN-domain are favored in the absence of bound coenzyme. The extent and nature of energy landscapes are therefore accessible through the integration of ELDOR spectroscopy with functional studies. We suggest this is a general approach that can be used to gain new insight into energy landscapes for biological ET mediated by conformational sampling mechanisms.

Introduction

The importance of conformational search mechanisms to enhance biological electron transfer (ET) in dynamic protein systems has been emphasized in recent years,[1−3] but little is known about the properties of the energy landscape associated with these reactions. A key question is whether these landscapes are smooth, enabling a stochastic and rapid search of energy space, or rugged, with consequent impact on the rate of sampling (and ET) and the potential for observing metastable states across the energy landscape. With small proteins (e.g., cytochrome *c*), electrostatic steering of the electron carrier enables limited exploration of conformational space in interactions with partner proteins.[4] By exploring multiple conformations there is increased opportunity for populating productive ET geometries.[5−7] A "rolling motion" over the surface of the partner protein enables a rapid search for reactive configurations through the principle of "reduction in dimensionality". This is supported by cross-linking in apparently optimal positions that can impede ET by restricting mobility.[8] Extensive conformational sampling mechanisms have been seen in complexes formed between primary dehydrogenases and electron transferring flavoproteins.[3,9,10] Here, domain motion in the assembled ET complex identifies reactive conformations through localized searches on the surface of the partner protein. Similar models have been proposed for intraprotein ET systems.[11−13] A notable example is the proposed "toggling" of the flavin mononucleotide (FMN)-domain of nitric oxide synthase required to optimize electronic coupling between the nicotinamide adenine phosphate dinucleotide (NADPH)/flavin adenine dinucleotide (FAD)-domain and the heme oxygenase domain.[14,15]

The structural similarity of cytochrome P450 reductase (CPR) enzymes[16] with nitric oxide synthases[14] suggests that confor-

‡ Current address: Department of Anatomy and Structural Biology and Gruss-Lipper Biophotonics Center, Albert Einstein College of Medicine, New York, NY 10661.

(1) Davidson, V. L. *Acc. Chem. Res.* **2000**, *33*, 87–93.
(2) Leys, D.; Scrutton, N. S. *Curr. Opin. Struct. Biol.* **2004**, *14*, 642–7.
(3) Toogood, H. S.; Leys, D.; Scrutton, N. S. *FEBS J* **2007**, *274*, 5481–504.
(4) Bashir, Q.; Volkov, A. N.; Ullmann, G. M.; Ubbink, M. *J. Am. Chem. Soc.* **2010**, *132*, 241–7.
(5) Crowley, P. B.; Ubbink, M. *Acc. Chem. Res.* **2003**, *36*, 723–30.
(6) Li, Q. S.; Schwaneberg, U.; Fischer, P.; Schmid, R. D. *Chemistry* **2000**, *6*, 1531–6.
(7) Mei, H.; Wang, K.; Peffer, N.; Weatherly, G.; Cohen, D. S.; Miller, M.; Pielak, G.; Durham, B.; Millett, F. *Biochemistry* **1999**, *38*, 6846–54.
(8) van Amsterdam, I. M.; Ubbink, M.; Einsle, O.; Messerschmidt, A.; Merli, A.; Cavazzini, D.; Rossi, G. L.; Canters, G. W. *Nat. Struct. Biol.* **2002**, *9*, 48–52.
(9) Leys, D.; Basran, J.; Talfournier, F.; Sutcliffe, M. J.; Scrutton, N. S. *Nat. Struct. Biol.* **2003**, *10*, 219–25.
(10) Toogood, H. S.; van Thiel, A.; Basran, J.; Sutcliffe, M. J.; Scrutton, N. S.; Leys, D. *J. Biol. Chem.* **2004**, *279*, 32904–12.
(11) Gruez, A.; Pignol, D.; Zeghouf, M.; Coves, J.; Fontecave, M.; Ferrer, J. L.; Fontecilla-Camps, J. C. *J. Mol. Biol.* **2000**, *299*, 199–212.
(12) Feng, C.; Kedia, R. V.; Hazzard, J. T.; Hurley, J. K.; Tollin, G.; Enemark, J. H. *Biochemistry* **2002**, *41*, 5816–21.
(13) Elliott, S. J.; McElhaney, A. E.; Feng, C.; Enemark, J. H.; Armstrong, F. A. *J. Am. Chem. Soc.* **2002**, *124*, 11612–3.

10.1021/ja1016206

mational sampling might underpin the mechanism of ET in these important redox systems. Human CPR is a membrane-bound modular flavoprotein containing FAD and FMN. CPR catalyzes ET from NADPH to cytochromes P450 in the endoplasmic reticulum[17] and has originated from the fusion of two ancestral genes encoding a FAD-binding ferredoxin-$NADP^+$ reductase and a FMN-containing flavodoxin.[18] The crystal structure of rat CPR[16] has revealed the organization of the flavin-binding domains, which are separated by a flexible peptide hinge. Studies of human CPR by small-angle X-ray scattering (SAXS) suggest the FMN-domain is flexible.[19] NADPH binds to the ferredoxin-$NADP^+$-reductase domain where it transfers hydride to the N5 of FAD followed by ET from FAD to FMN.[16,20−22] Transient association of CPR with P450 enables the flavin cofactors to mediate the successive transfer of two electrons from a two-electron donor, NADPH, to the obligatory one-electron acceptor moiety (the heme) in the P450s.

The $NADP^+$-bound crystal structure of rat CPR has revealed a short edge-to-edge distance of 3.9 Å between the flavin isoalloxazine C8 methyl carbons.[16] This short distance is expected to result in a very fast and efficient ET between the flavin cofactors (up to 10^{10} s^{-1} using Dutton's ruler[23−25]). Interflavin ET is however slow in CPR. Temperature-jump (T-jump) relaxation experiments established that interflavin ET of NADPH-reduced human CPR occurs with an observed rate constant of ∼55 s^{-1},[26] and comparable rates have been measured using laser flash photolysis, which yielded an interflavin ET rate from $FADH^\bullet$ to $FMNH^\bullet$ of ∼36 s^{-1}.[27] Gating of internal ET in human CPR through a rate-limiting conformational change has been suggested from T-jump studies,[26,28] consistent with the expanded molecular envelope seen for the FMN-domain in SAXS studies[19] and a more open conformation inferred from crystallographic analysis of mutant[29] and chimeric[30] forms of CPR. This proposed conformational control is an additional feature in the complex ET mechanism, involving pH[31] and solvent[31] gating of the relaxation to the thermodynamic equilibrium for the two-electron reduced species (quasi-equilibrium (QE) state in Scheme 1) and long-range ligand effects on CPR conformation and energy propagation.[32,33] Here, we investigate the landscape for motions implicated in the conformational gating of interflavin ET in human CPR by electron-electron double resonance (ELDOR) spectroscopy. We also examine the effects of exploring this landscape by pressure perturbation, and by changes in solvent viscosity and ionic strength, on the observed rates of interflavin ET.

Scheme 1. Simplified Reductive Half-Reaction of Human Cytochrome P450 Reductase[a]

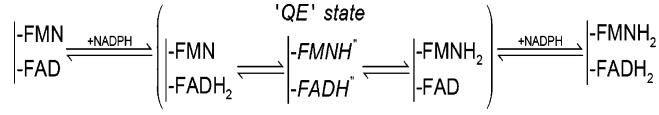

[a] Adapted from ref 31. The di-radical species in italics is uniquely monitored both by ELDOR and optically at 600 nm.

Materials and Methods

All materials were obtained from Sigma-Aldrich (Dorset, U.K.), except NADPH (Melford Laboratories, Chelsworth, U.K.). Intact human CPR was purified essentially as described previously.[34,35] CPR purification and sample preparation was conducted in a Belle Technology glovebox under a nitrogen atmosphere. Buffers were made anaerobic by bubbling with nitrogen for at least 20 min and transferred into the glovebox; the bottles were then left open in the glovebox overnight to achieve complete equilibration with the anaerobic atmosphere. Oxygen levels were kept below 2 ppm throughout the experiment.

The enzyme was purified in a partially reduced form and had to be oxidized prior to each experiment by adding a few grains of the oxidant potassium ferricyanide. This was performed within the anaerobic box. The protein solution was applied immediately onto a Pharmacia (Leatherhead, UK) PD-10 gel filtration column pre-equilibrated with the desired anaerobic buffer. Thus, this step resulted in the removal of ferricyanide as well as achieving the transfer of CPR into the required anaerobic buffer system. The CPR concentration was then determined using an extinction coefficient of $\epsilon_{454\ nm} = 22\ mM^{-1}\ cm^{-1}$ for the oxidized enzyme.[36] Production of the diradical (disemiquinoid) form of CPR was by the addition of a stoichiometric equivalent of NADPH or by reductive titration against dithionite under anaerobic conditions as described.[31,34]

All EPR spectra were obtained using a Bruker ELEXSYS E500/E580 spectrometer operating at X-band. Temperature control was effected using an Oxford Instruments ESR900, for continuous wave EPR, or ESR935, for pulsed measurements, cryostat connected to an ITC503 temperature controller. Continuous wave spectra were obtained at 80K using the parameters given in the figure captions. Two pulse echo decays[37] were obtained using a $\pi/2-\tau-\pi-\tau$-acquire sequence with a 32 ns π pulse length and τ starting at 200 ns using 1024 8 ns increments. Pulsed field swept EPR spectra[37] were obtained using soft pulses in order to avoid excitation bandwidth-induced spectrum broadening. The $\pi/2$-$\tau-\pi$-τ-acquire pulse sequence was employed, with $\pi = 200$ ns and $\tau = 1$ μs.

(14) Garcin, E. D.; Bruns, C. M.; Lloyd, S. J.; Hosfield, D. J.; Tiso, M.; Gachhui, R.; Stuehr, D. J.; Tainer, J. A.; Getzoff, E. D. *J. Biol. Chem.* **2004**, *279*, 37918–27.
(15) Dunford, A. J.; Rigby, S. E.; Hay, S.; Munro, A. W.; Scrutton, N. S. *Biochemistry* **2007**, *46*, 5018–29.
(16) Wang, M.; Roberts, D. L.; Paschke, R.; Shea, T. M.; Masters, B. S.; Kim, J. J. *Proc. Natl. Acad. Sci. U. S. A.* **1997**, *94*, 8411–6.
(17) Iyanagi, T.; Mason, H. S. *Biochemistry* **1973**, *12*, 2297–308.
(18) Porter, T. D.; Kasper, C. B. *Biochemistry* **1986**, *25*, 1682–7.
(19) Ellis, J.; Gutierrez, A.; Barsukov, I. L.; Huang, W.-C.; Grossmann, J. G.; G. C. K., R. *J. Biol. Chem.* **2009**, *284*, 36628–36637.
(20) Vermilion, J. L.; Coon, M. J. *J. Biol. Chem.* **1978**, *253*, 8812–9.
(21) Vermilion, J. L.; Ballou, D. P.; Massey, V.; Coon, M. J. *J. Biol. Chem.* **1981**, *256*, 266–77.
(22) Shen, A. L.; Porter, T. D.; Wilson, T. E.; Kasper, C. B. *J. Biol. Chem.* **1989**, *264*, 7584–9.
(23) Marcus, R. A.; Sutin, N. *Biochim. Biophys. Acta* **1985**, *811*, 265–322.
(24) Moser, C. C.; Keske, J. M.; Warncke, K.; Farid, R. S.; Dutton, P. L. *Nature* **1992**, *355*, 796–802.
(25) Page, C. C.; Moser, C. C.; Chen, X.; Dutton, P. L. *Nature* **1999**, *402*, 47–52.
(26) Gutierrez, A.; Paine, M.; Wolf, C. R.; Scrutton, N. S.; Roberts, G. C. *Biochemistry* **2002**, *41*, 4626–37.
(27) Bhattacharyya, A. K.; Hurley, J. K.; Tollin, G.; Waskell, L. *Arch. Biochem. Biophys.* **1994**, *310*, 318–24.
(28) Gutierrez, A.; Munro, A. W.; Grunau, A.; Wolf, C. R.; Scrutton, N. S.; Roberts, G. C. *Eur. J. Biochem.* **2003**, *270*, 2612–21.
(29) Hamdane, D.; Xia, C.; Im, S. C.; Zhang, H.; Kim, J. J.; Waskell, L. *J. Biol. Chem.* **2009**, *284*, 11374–84.
(30) Aigrain, L.; Pompon, D.; Morera, S.; Truan, G. *EMBO Rep.* **2009**, *10*, 742–7.
(31) Brenner, S.; Hay, S.; Munro, A. W.; Scrutton, N. S. *FEBS J.* **2008**, *275*, 4540–57.
(32) Grunau, A.; Paine, M. J.; Ladbury, J. E.; Gutierrez, A. *Biochemistry* **2006**, *45*, 1421–34.
(33) Grunau, A.; Geraki, K.; Grossmann, J. G.; Gutierrez, A. *Biochemistry* **2007**, *46*, 8244–55.
(34) Munro, A. W.; Noble, M. A.; Robledo, L.; Daff, S. N.; Chapman, S. K. *Biochemistry* **2001**, *40*, 1956–63.
(35) Smith, G. C.; Tew, D. G.; Wolf, C. R. *Proc. Natl. Acad. Sci. U. S. A.* **1994**, *91*, 8710–4.
(36) Gutierrez, A.; Lian, L. Y.; Wolf, C. R.; Scrutton, N. S.; Roberts, G. C. *Biochemistry* **2001**, *40*, 1964–75.
(37) Schweiger, A.; Jeschke, G. *Principles of Pulse Electron Paramagmetic Resonance*; Oxford University Press: Oxford, U.K., 2001; pp 183−9, 226−9, 420−1.

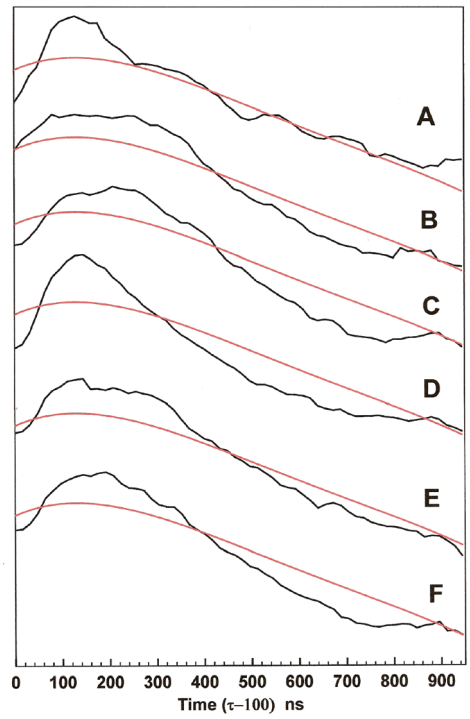

Figure 1. Raw four pulse ELDOR traces together with the third order polynomial functions used to baseline the data (red). A, $NADP^+$-bound CPR in low salt buffer; B, CPR in low salt buffer; C, 2′,5′-ADP-bound CPR in low salt buffer; D, $NADP^+$-bound CPR in 500 mM KCl-containing buffer; E, CPR in 500 mM KCl-containing buffer; F, 2′,5′-ADP-bound CPR in 500 mM KCl-containing buffer.

Four pulse ELDOR spectra[37] were recorded using a $\pi/2-T-\pi-T+\tau-\pi-\tau$-acquire sequence with $T = 200$ ns and $\tau = 960$ ns. The π pulse length was 32 ns. The "fourth" pulse, a π pulse applied at the pump microwave frequency, was incremented in 16 ns steps during the $T + \tau$ period starting at 100 ns after the second π pulse. The interval τ was limited to 960 ns because of the spin−spin relaxation, phase memory time T_M, of the flavosemiquinones, which precluded detection of the refocused echo at longer values of τ. If the timing of the fourth pulse is indicated as $t = 0$ at 100 ns after the second π pulse and t is incremented thereafter, the modulation of the four pulse ELDOR echo is given by $V_{4p}(t) = \cos(\omega_{ee}(t - T))$,[37] where ω_{ee} is the electron−electron coupling. All pulse experiments were recorded at 80K and at a repetition frequency of 200 Hz because of the long electron spin−lattice relaxation time of the flavosemiquinone radical. Attempts to prolong τ by lowering the temperature and thus lengthening T_M were prohibited by the impact on the repetition rate (governed by the electron spin−lattice relaxation time T_{1e}), which lead to prohibitively slow repetition rates. Interelectron dipolar couplings were determined using Fourier transform of the baseline corrected four pulse ELDOR data to produce dipolar spectra. The raw ELDOR data were baseline corrected using a third-order polynomial, Figure 1, then a Hamming window function was applied in order to increase signal-to-noise following the subsequent Fourier transform and drive the decay function to completion, thus avoiding truncation effects. Each data set was then zero-filled to 1024 point prior to Fourier transformation. Tikhonov regularization[38] was not employed as the flavin cofactors have no motion independent of the movement of their binding domains and the measured distances are interpretable in terms of a simple physical model.

Stopped-flow experiments at ambient pressure were performed, essentially as described previously,[31] under anaerobic conditions with an Applied Photophysics SC18MV stopped-flow instrument housed in a glovebox. High-pressure stopped-flow experiments were performed using a Hi-Tech Scientific HPSF-56 high-pressure stopped-flow spectrophotometer (TgK Scientific, Bradford on Avon, UK), and 5−10 units mL^{-1} glucose oxidase and 50 mM glucose were added to make the samples anaerobic,[39,40] The two rate constants k_1 and k_2 were determined by either fitting traces measured at 600 nm to a double-exponential function, or were deconvoluted by global analysis of diode array data using an A → B → C model. Both methods produced equivalent results. The CPR concentration was typically ~20 μM and a 20-fold excess of NADPH was used. Comparable rates were also obtained in a high pressure experiment using a 10-fold excess of NADPH, indicating that neither k_1 nor k_2 are limited by NADPH binding and the reaction is essentially pseudofirst order.

Results and Discussion

Measuring Radical Separation in Disemiquinoid CPR. The reductive half-reaction of CPR is complex (Scheme 1; ref [31]). If CPR is reduced with two electrons, either by the addition of a stoichiometric equivalent of NADPH (the K_m is ~1 μM[28]) or equivalent dithionite, a kinetic or thermodynamic quasi-equilibrium mixture of states is formed (Scheme 1). Only one of these, the diflavosemiquinonoid (diradical) species, is EPR-detectable. We used ELDOR spectroscopy of two-electron reduced human CPR to measure distances between the FAD and FMN centers and to investigate the properties of the energy landscape for domain motion. Using the ELDOR method, we also probed the effects of ionic strength and ligand binding ($NADP^+$ and ADP) on the energy landscape for domain motion, since the influence of both salt and cofactors on the kinetics of interflavin ET has previously been demonstrated.[26,28]

The dipole−dipole coupling between the two electronic magnetic moments of the flavin semiquinone centers is related to the distance between them by the eq 1[37]

$$\nu_{DD}(\theta, r) = \frac{g_1 g_2 \mu_0 \mu_B^2}{4\pi h} \frac{1}{r^3}(3\cos^2\theta - 1) \qquad (1)$$

where g_1 and g_2 are the g values of the two spins, r is the distance between them, and θ is the angle between the interspin vector and the applied magnetic field. Therefore, determination of the dipole−dipole coupling between the two flavosemiquinones of CPR provides a means of quantitating differences in interflavin distance brought about by ligand binding. The four pulse ELDOR experiment provides a means of determining such dipole−dipole couplings. However, it has only been applied to a pair of flavosemiquinones once,[41] and this was in a dimeric protein wherein each monomer contained one flavosemiquinone, fixed relative to one another and having the same midpoint potential.

To set up the ELDOR experiment, it is necessary to first determine some parameters, notably the T_{1e} of the unpaired electrons, which determines the rate at which individual data points can be acquired without saturation, and the decay of the nuclear modulation in the electron spin echo. Figure S1 in the Supporting Information shows the results of two pulse echo decay experiments on CPR under six different experimental

(38) Tychonoff, A. N. *Sov. Math.* **1963**, *4*, 1035–1038.
(39) Pudney, C. R.; McGrory, T.; Lafite, P.; Pang, J.; Hay, S.; Leys, D.; Sutcliffe, M. J.; Scrutton, N. S. *ChemBioChem* **2009**, *10*, 1379–84.
(40) Hay, S.; Sutcliffe, M. J.; Scrutton, N. S. *Proc. Natl. Acad. Sci. U. S. A.* **2007**, *104*, 507–12.
(41) Kay, C. W.; Elsasser, C.; Bittl, R.; Farrell, S. R.; Thorpe, C. *J. Am. Chem. Soc.* **2006**, *128*, 76–7.

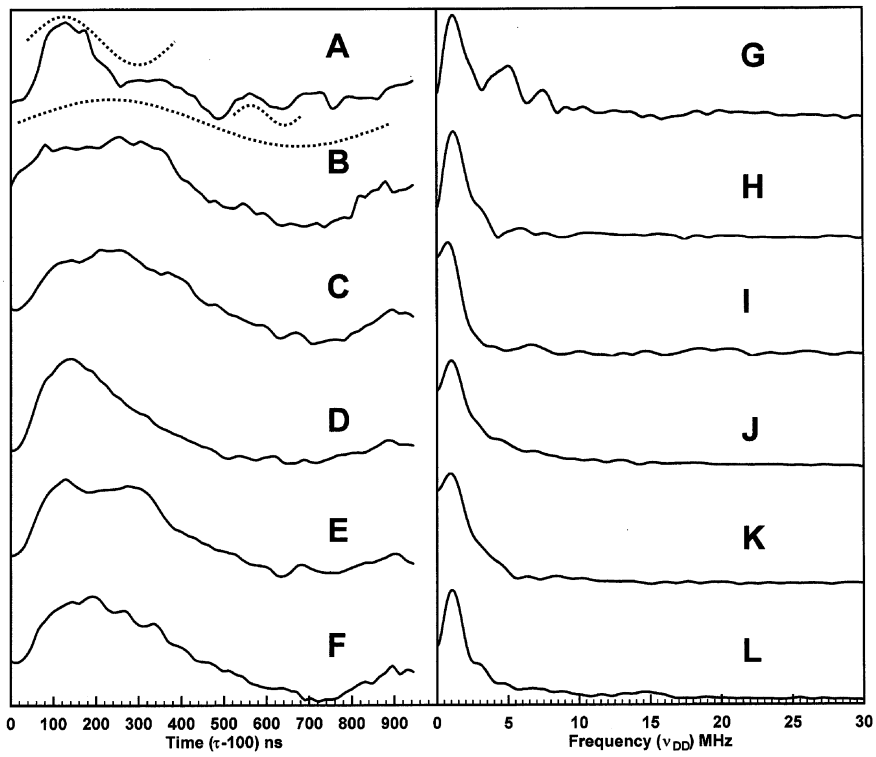

Figure 2. Baseline corrected four pulse ELDOR time traces, A−F, and the conjugate Fourier transforms of those time traces, G−L, of the disemiquinone oxidation state of human CPR. A and G, $NADP^+$-bound CPR in low salt buffer; B and H, CPR in low salt buffer; C and I, 2′,5′-ADP-bound CPR in low salt buffer; D and J, $NADP^+$-bound CPR in 500 mM KCl-containing buffer; E and K, CPR in 500 mM KCl-containing buffer; F and L 2′,5′-ADP-bound CPR in 500 mM KCl-containing buffer. Dotted lines around A illustrate the three components with differing oscillation frequencies present in that time trace. Calculated interflavin distances are given in Table 1.

conditions. All the traces show that the deep modulations that arise from hyperfine coupling to ^{14}N nuclei have decayed away after 1 μs, while the overall exponential decay continues and can be fitted with a monoexponential function giving an approximate T_M for the flavosemiquinones of 1.2 μs. Thus, sufficient signal remains after 1 μs to allow for the collection of ELDOR data free of nuclear modulation effects. To determine the appropriate positions for pump and detection frequencies, pulsed field swept spectra were obtained using a soft two-pulse echo (Figure S2, Supporting Information). The pump and detection frequencies were placed symmetrically about the intensity maximum of the field swept spectrum and separated by 70 MHz, with the pump pulse at the higher field (lower frequency). Figure 1 shows the raw data, echo integral variation with time, from the four pulse ELDOR experiments together with fits to a third-order polynomial baseline. Following baseline subtraction, the results of these experiments in both time domain and in frequency domain, after Fourier transformation (essentially one-half of the dipolar spectrum), are shown in Figure 2. Trace A, from $NADP^+$-bound CPR in low salt buffer, is obviously composed of oscillations at several frequencies, marked on the figure, and the conjugate Fourier transform, trace G, shows three major frequency components. These correspond to the perpendicular components ($\theta = 90$) of the dipolar powder (Pake) pattern.[37] The much weaker parallel components, which exhibit only ~10% of the intensity of the perpendicular components, are not clearly observed in these spectra; therefore, we have not assigned features to them even though there are possible candidates. They are not required for distance determination. Each of these frequencies corresponds to a discrete dipolar coupling, ν_{DD}, and thus through eq 1 to three discrete interflavin distances, 36.1, 21.6, and 19.0 Å. Traces B and C, together with their Fourier transforms traces H and I, show only one major oscillation at frequencies that correspond, through the same reasoning applied to trace A, to interflavin distances of 36.1 and 40.2 Å, respectively (Table 1).

Table 1. Inter-Flavin Distance Measured Using ELDOR

ligand	[KCl] (mM)	distance (Å)	trace[a]
$NADP^+$	0	19.0, 21.6, 36.1	A, G
	0	36.1	B, H
2′,5′-ADP	0	40.2	C, I
$NADP^+$	500	15.4−25.8[b], 37.2	D, J
	500	19.2−25.8[b], 37.2	E, K
2′,5′-ADP	500	19.2−25.8[b], 37.2	F, L

[a] ELDOR traces in Figure 2. [b] A continuum of distances was measured rather than discrete values.

The addition of 500 mM potassium chloride to the protein solution gives rise to rather similar 4-pulse ELDOR results in all three states of the protein examined, as shown in Figure 2 traces D, E, and F and their conjugate Fourier transforms, J, K, and L, respectively. In each case, the ELDOR data clearly cannot be approximated by a small number of simple sinusoidal functions as the apparent wavelength varies during each oscillation. This suggests a superposition of many frequencies within this data. However, this is not at first obvious in the Fourier transforms. Each of these gives rise to a single Gaussian line at ν_{DD} of 1 MHz, corresponding to an interflavin distance of 37.2 Å. This is consistent with the distances estimated from the 4-pulse ELDOR of the low salt samples, both the sample containing 2′,5′-ADP and that without effectors. Problematically, such a distance is clearly inconsistent with the behavior of the

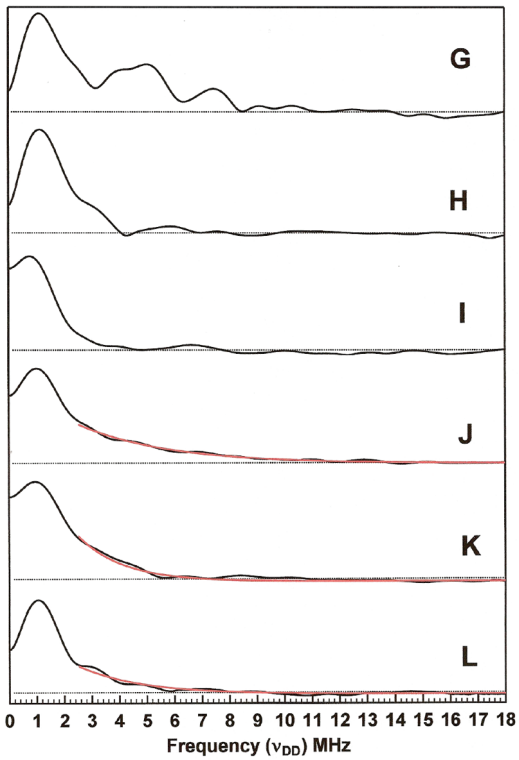

Figure 3. Expansions of the Fourier transformed, frequency domain, spectra of Figure 2 showing monoexponential fits (red), described in the text, to the three spectra obtained in 500 mM KCl-containing buffer, J, K and L. Dotted lines show linear baselines fitted to each of the spectra. G, $NADP^+$-bound CPR in low salt buffer; H, CPR in low salt buffer; I, 2′,5′-ADP-bound CPR in low salt buffer; J, $NADP^+$-bound CPR in 500 mM KCl-containing buffer; K, CPR in 500 mM KCl-containing buffer; L 2′,5′-ADP-bound CPR in 500 mM KCl-containing buffer.

$NADP^+$-bound CPR under low salt conditions. Closer inspection of the Fourier transforms J, K, and L reveals the origin of this inconsistency, Figure 3. These Fourier transforms cannot be approximated by a few simple Gaussian lineshapes alone but rather reveal a long "tail" to high frequency of the more obvious Gaussian line. This 'tail' can be approximated by an exponential distribution of distances, but it may consist of discrete, rather than continuous, data and could be formed from the overlap of an unknown number of discrete Gaussian lines. If such discrete states exist, they may not be resolvable because of the line-widths of lines in the Fourier transform which are dictated by the decay of the time-dependent modulation. The half height line widths of lines in the frequency domain, Fourier transformed, data are 1.2−1.4 MHz. It is difficult to resolve lines separated by less than 1/4 of the half height line width. Thus if the tails do consist of discrete data there must be at least 30 discrete, evenly spaced lines present for them to be separated by less than 0.3−0.35 MHz and thus be unresolved. Whether there are 30 states, many more, or a continuum we cannot determine from our experiments. Nevertheless, the simple exponential fitting analysis shows that in the $NADP^+$-bound form the exponential distribution is centered on a ν_{DD} of 3.0 MHz, corresponding to a distance of 25.8 Å, and extends to ν_{DD} of 14.1 MHz, corresponding to a distance of 15.4 Å. Where 2′,5′-ADP is bound to CPR or the protein is simply reduced without substrate/ligand present, the distribution is centered around a ν_{DD} of 1.8 MHz, corresponding to a distance of 25.8 Å and extends to a ν_{DD} of 7.3 MHz, corresponding to a distance of 19.2 Å (Table 1). This assumes that we observe only contributions from the intense perpendicular components of the dipolar coupling, which seems reasonable as even the parallel component of the Gaussian line at low ν_{DD} would be too weak, based on the reported order of magnitude difference in intensity between parallel and perpendicular components,[41] to contribute to the tail.

Extensive Sampling of Conformational Space in CPR. Our EPR data show that low-temperature pulsed ELDOR spectroscopy can be applied to study dynamic events in the diflavin protein human cytochrome P450 reductase. The results quantitate $NADP^+$-dependent changes in interflavin distance within wild-type reductase for the first time. However, it is important to understand the nature and limitations of the results. The flavin cofactor, unlike some of the artificially introduced nitroxide spin labels employed in pulsed ELDOR studies, has essentially no motion independent of the protein to which it is attached. Thus our results indicate that movement of either the FAD or FMN domains of CPR occurs upon the binding of $NADP^+$. Within our current understanding of the structure of CPR,[16] movement of the FMN-binding domain seems most likely.[19,32] While this may be consistent with other, room-temperature, measurements the experimental temperature employed in the pulsed ELDOR experiments must be taken into account. At 80 K, the lack of thermal energy will prevent domain motion, and such immobility will be further reinforced by the ordering of solvent water into the ice (Wurtz) structure.[42] Furthermore, since each sample took several seconds to freeze, thermodynamic equilibrium between possible conformations will have been established at the lowest temperature that allows for domain motion. Thus the ELDOR results represent the conformational distributions exhibited by the protein just before motion ceased because of lack of thermal energy, those conformations that exist at the bottom of thermodynamic wells or minima.

While the data can be taken comparatively as a measure of relative interflavin distance within CPR, the actual distance being measured should be considered. The unpaired electron is delocalized over all three rings of the flavosemiquinone structure. Thus the distances measured do not represent distances between points, but rather the distances between a weighted mean of the unpaired electron spin density distribution over the flavosemiquinone. The center of such a distribution lays essentially at C(4a).[43] Furthermore, even where the unpaired electron spin density distribution of a flavosemiquinone varies with the binding of substrates, inhibitors or other effectors close to it, the center of the distribution remains at C(4a). This approximation has therefore been used in previous studies involving pulsed ELDOR of flavin semiquinones.[41,48] The critical distance for ET between flavin cofactors is likely to be edge-to-edge distance. According to the published crystal structures of wild-type rat CPR showing short interflavin distances,[16] the shortest edge-to-edge distance is between the methyl group-bearing edge of the dimethylbenzene moieties of the flavin cofactors. This edge is some 4.7 Å from C(4a) and the methyl groups are likewise at a mean distance of 6.15 Å from C(4a). Thus the measured closest distance of 19 Å measured for CPR in low ionic strength conditions with bound $NADP^+$ (Table 1) would leave the flavin methyl groups only 6.7 Å apart, and the potentially closest distance of 15.4 Å

(42) Ansari, A.; Jones, C. M.; Henry, E. R.; Hofrichter, J.; Eaton, W. A. *Science* **1992**, *256*, 1796–8.
(43) Weber, S.; Mobius, K.; Richter, G.; Kay, C. W. *J. Am. Chem. Soc.* **2001**, *123*, 3790–8.

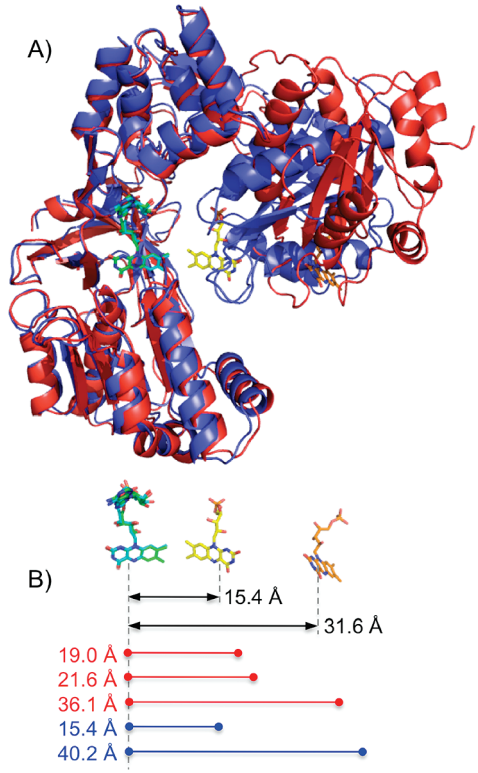

Figure 4. (A). X-ray crystal structures of CPR (PDB 1AMO; blue) and the "open" ΔTGEE CPR mutant (molecule A of PDB 3ES9; red), aligned over all FAD heavy atoms. The FAD molecules are shown in the same color as the ribbons, while the FMN molecules are shown in yellow (wild-type) and orange (ΔTGEE). (B). The distance between the FAD and FMN C(4a) atoms in the two crystal structures in panel A. Distances measured using ELDOR for $NADP^+$-bound CPR in the absence of KCl are shown to scale in red, and the minimum and maximum distances measured (Table 1) are shown in blue.

inferred from the ν_{DD} distribution in 500 mM potassium chloride with $NADP^+$ bound would leave the methyl groups only 3.1 Å apart, essentially in van der Waals contact.

These interflavin distances can be further compared to the two published structures of CPR, the wild-type "closed"[16] and ΔTGEE mutant "open"[29] structures (Figure 4). These structures show the FAD and FMN-binding domains of CPR separated by a hinge domain (residues 232−244[16]). The open conformation appears to be formed when the FMN domain rotates about this hinge, increasing the separation between the FAD and FMN C(4a) atoms from 15.4 Å in the closed conformation to 31.6 Å in the open conformation. While these values are remarkably similar to those measured here using ELDOR (Table 1), we did, in some cases, measure slightly larger distances than is observed in the "open" structure. However, there are three CPR molecules found within the asymmetric packing unit of the "open" structure,[29] each in a distinct conformation. The two other conformations not shown in Figure 4 have more extended structures, with longer interflavin distances, but incomplete electron density around the FMN that prevents the measurement of the actual C(4a) separation.

In summary, the range of interflavin distances we have measured using ELDOR (Table 1) are in excellent agreement with those distances observed in the available crystal structures of CPR (Figure 4). Further, the ELDOR data suggest that an equilibrium distribution of multiple extended open and compact closed conformations is found in solution. The landscape linking these states would appear to be 'frustrated', allowing the trapping of certain conformations upon crystallization or freezing (as in the case of the ELDOR samples). The binding of $NADP^+$ to CPR favors conformations with shorter interflavin distances relative to the unliganded protein, two such distances being associated with apparent energy minima and therefore giving rise to resolved dipolar couplings in the ELDOR Fourier transforms. Furthermore the ELDOR data also suggest that this landscape is perturbed by the addition of 500 mM KCl. Under such conditions the equilibrium distribution of states shifts to favor more compact conformations compared to those exhibited by CPR in the absence of KCl, shorter interflavin distances with larger dipolar coupling, see Table 1, while also becoming less "frustrated" in having fewer distinct conformations, with resolved dipolar coupling, that can be thermodynamically trapped. We next tested this idea my characterizing the observed interflavin ET solution kinetics.

Functional Exploration of the Landscape by Pressure and Solvent Perturbation. Hydrostatic pressure can be used to perturb an equilibrium distribution of conformational states that comprise the free energy landscape for an enzyme-catalyzed reaction,[39,40] and we extend this approach here to studies of conformationally coupled ET in human CPR. We initially performed solvent-accessible surface area calculations on the open and closed CPR crystal structures (Table S4, Supporting Information) and estimate that moving from the closed to open conformation shown in Figure 4 exposes an additional 840 $Å^2$ of CPR surface area to solvent, approximately a 3% increase. No large internal cavities (voids) were observed in any of the calculations. The number of additional water molecules (Δn_w) that will bind to the enzyme can be then be estimated to be ~65 by $\Delta n_w = \Gamma \Delta SA$, where ΔSA is the change in surface area and Γ is the protein surface density of water (0.0775 water molecules/$Å^2$).[44] The water surface density has been estimated[44] to be 1.6−2.0 $cm^3\ mol^{-1}$, so the volume of the CPR/bound water sphere would be expected to increase by 100−130 $cm^3\ mol^{-1}$ upon moving from a closed to open conformation. Consequently, we would expect increasing pressure to favor more compact enzyme conformations with reduced volumes, that is, the closed form.

As interflavin ET in CPR is likely to be conformationally gated, the observed rate of ET can be modeled using absolute rate theory, unlike a true ET reaction, which is best modeled using the nonadiabatic description of Marcus theory.[23] The pressure (p)-dependence of an observed rate constant is described using absolute rate theory by assuming a quasi-equilibrium between the reactant and transition state[45,46]

$$k_{obs}(p, T) = k_0 \exp(-\Delta V^{\ddagger} p/R_p T + \Delta\beta^{\ddagger} p^2/2R_p T) \qquad (2)$$

where $R_p = 83.13\ cm^3\ mol^{-1}$ bar K^{-1}, k_0 is the observed rate constant extrapolated to 0 bar, $\Delta V^{\ddagger}$ is the apparent difference between the volume of the reactant and transition states, and $\Delta\beta^{\ddagger}$ is the compressibility of the transition state: $\Delta\beta^{\ddagger} = d\Delta V^{\ddagger}/dp$. We used high-pressure stopped-flow spectroscopy to study the kinetics of hydride transfer from NADPH to FAD and ET from FAD to FMN, by monitoring the formation and decay of the blue (protonated) disemiquinoid form of CPR, following mixing of oxidized enzyme with (typically 20-fold) excess

(44) Webb, J. N.; Webb, S. D.; Cleland, J. L.; Carpenter, J. F.; Randolph, T. W. *Proc. Natl. Acad. Sci. U. S. A.* **2001**, *98*, 7259–7264.
(45) Gladstone, S.; Laidler, K. J.; Eyring, H. *The Theory of Rate Processes*; McGraw-Hill: New York, 1941.
(46) Northrop, D. B. *J. Am. Chem. Soc.* **1999**, *121*, 3521–3524.

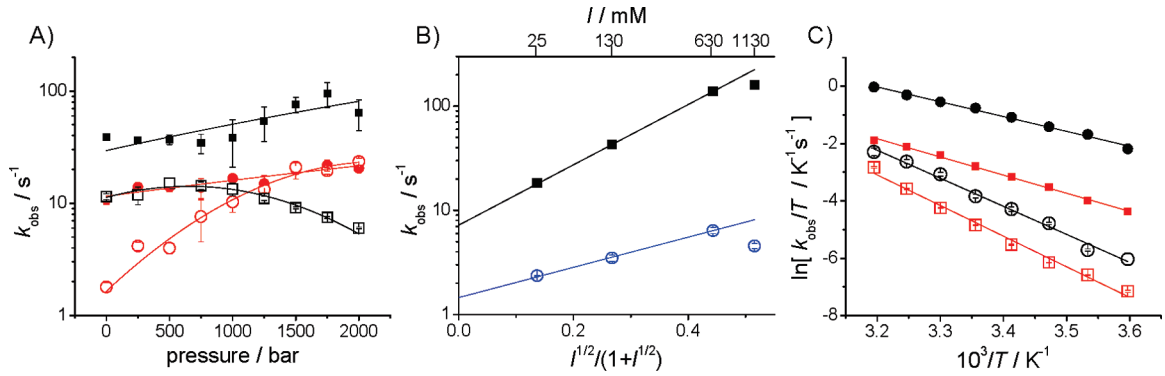

Figure 5. ET solution kinetics for human CPR. (A). The hydrostatic pressure dependence of k_1 (filled symbols) and k_2 (open symbols) measured at 25 C in the presence (black) and absence (red) of 500 mM KCl. The data are fit to eq 2 and the $\Delta V^{\ddagger}$ and $\Delta\beta^{\ddagger}$ values are given in Table S1, Supporting Information. (B). The ionic strength (I)-dependence of k_1 (black) and k_2 (blue) measured at 25 C. The data (excluding the $I = 1130$ mM point) are fit to eq 3. (C). Eyring plots showing the temperature dependence of k_1 (filled symbols) and k_2 (open symbols) measured when $I = 25$ mM (red) and $I = 630$ mM (black). The $\Delta H^{\ddagger}$ and $\Delta S^{\ddagger}$ values are given in Table S3, Supporting Information. Experimental conditions: High pressure measurements were performed in 50 mM Tris-HCl, pH 7.5. All other experiments were performed in potassium phosphate buffer, pH 7.5. The ionic strength was achieved by varying the buffer ($I = 25-133$ mM) and KCl concentration ($I > 133$ mM).

NADPH (Scheme 1; Figure S3, Supporting Information).[36] Clearly, observed rate constants measured in stopped-flow studies represent the approach to an equilibrium distribution of multiple enzyme species. Broadly, the observed rate constant k_1 (increase in absorption at 600 nm) reports on initial enzyme reduction by NADPH to generate the $FADH_2$ state, and the subsequent internal ET to establish the QE state in Scheme 1. The QE distribution includes the disemiquinoid ($FADH^{\bullet}$ $FMNH^{\bullet}$) state, which accounts for the absorption increase at 600 nm (Figure S3, Supporting Information). The observed rate constant k_2 represents reduction predominantly to the four-electron ($FADH_2$ $FMNH_2$) reduced state following transfer of a second hydride from NADPH to CPR (Scheme 1), leading to a collapse in absorption at 600 nm (Figure S3, Supporting Information). Reaction traces measured at 600 nm are therefore biphasic and monitor the formation and decay of the $FADH^{\bullet}$ $FMNH^{\bullet}$ state and k_1 and k_2 can be determined by fitting these data to a double-exponential function.

The reactions were performed under pseudo-first-order conditions, with both observed rate constants, k_1 and k_2, independent of NADPH concentration. Both k_1 and k_2 increase with increasing pressure (Figure 3A; Table S1, Supporting Information), consistent with an altered and more functionally favored distribution of conformational states across the energy landscape for interflavin ET at high pressure. Although the pressure data do not provide direct information on the nature of the structural change as a result of perturbing the equilibrium distribution of conformational states (i.e., the energy landscape), the pressure dependence of both k_1 and k_2 is likely attributed to CPR adopting a higher population of closed and ET-competent/"reaction-ready" conformations at high pressure compared with those at 1 bar, as predicted by the surface area calculations described above. The decrease in k_2 at pressure >1 kbar, may arise from a "freezing out" of some of the productive conformational sampling of the FMN domain, that is, very high pressure traps the enzyme in a nonoptimal conformation. Although there are difficulties in gaining detailed structural insight from the pressure data alone, the pressure related changes to k_1 and k_2 indicate a change in the conformational distribution across the energy landscape. This indicates that conformational sampling is an integral part of the (gated) ET mechanism in CPR, thereby demonstrating the relevance of our ELDOR studies, and the rugged energy landscape at low salt concentrations inferred from these studies, to the ET function of the enzyme. The dependence of k_1 and k_2 on the viscosity of the bulk medium (both k_1 and k_2 decrease with increasing viscosity) also points to a key role for conformational sampling in facilitating ET between the flavins in human CPR (Figure S4 and Table S2, Supporting Information).

As the high-salt ELDOR experiments (Figure 2, Table 1) suggest that increasing ionic strength alters the conformational sampling of CPR, we also explored the ionic strength dependence of k_1 and k_2 by performing stopped-flow reactions as a function of ionic strength at atmospheric pressure (Figure 5B). The ionic strength data were fit to eq 3

$$\log_{10} k_{obs}(I) \approx \log_{10} k_0 + z_A z_B(\sqrt{I}/(1 + \sqrt{I})) \qquad (3)$$

which is derived by combining the Brønsted-Bjerrum and the extended law of Debye−Hückel and is used for high ionic strengths.[47] This relationship was developed for bimolecular reactions and should only be used for comparison in this study. If the charges z_A and z_B are of the equal sign (i.e., either positive or negative), then there is an increase in k_{obs} with increasing ionic strength, I. The ionic strength dependence measurements were made at varying temperatures between 5 and 40 C (Figure 5C; Table S3, Supporting Information). Both rate constants satisfy the ionic strength dependence indicated by eq 3 and $z_A z_B$ does not significantly change with temperature, with values of 2.8 ± 0.3 and 1.5 ± 0.4 for k_1 and k_2, respectively. Additionally, both k_1 and k_2 maintain their viscosity dependence (Figure S3 and Table S2, Supporting Information) at high ionic strength, suggesting that interflavin ET is still conformationally gated in high salt. Increasing the ionic strength lowers the enthalpic barrier to k_1 and increases the negative activation entropy (Figure 5C; Table S3, Supporting Information). This is consistent with k_1 being (at least partially) gated by motion of the FMN-domain, which under high ionic strength conditions more favorably redistributes to closed and reactive conformers from the more extended $NADP^+$-free distribution seen in the ELDOR (disemiquinoid enzyme) and SAXS[19] (oxidized enzyme) studies. The magnitude of the (negative) activation entropy increases

(47) Carstensen, J. T. *J. Pharm. Sci.* **1970**, *59*, 1140–1143.
(48) Swanson, M. A.; Kathirvelu, V.; Majtan, T.; Frerman, F. E.; Eaton, G. R.; Eaton, S. S. *J. Am. Chem. Soc.* **2009**, *131*, 15979–15979.

with increasing ionic strength (Table S3, Supporting Information). This increase is also consistent with a redistribution from a more disordered (open) to more ordered (closed) reactant state in the presence of high salt. Thus, at high ionic strength the FMN-domain is able to either sample more conformations (some with a slightly shorter interflavin distance as seen by EPR), or sample these conformations more readily/quickly, thus enhancing k_1. Either scenario is consistent with the trend in activation entropy, which becomes more negative as the ionic strength is increased.

The rate enhancement of k_2 by increasing ionic strength is not as significant, but is broadly consistent with the model advanced for k_1. We emphasize, however, that k_2 captures a number of additional steps in the reaction mechanism (e.g., $NADP^+$ release prior to NADPH binding and transfer of a second hydride anion; Scheme 1) which might complicate the analysis in terms of FMN-domain motion. The main point to note is that by raising the ionic strength of the bulk solvent, there is an increase in the observed rate of ET (k_1 and k_2). This points to an overall shielding from net electrostatic charge similarity, which favors conformations that are 'reactive' for ET. As indicated by our ELDOR studies, high ionic strength affects the equilibrium distribution across the energy landscape, favoring (through electrostatic shielding) those closed conformations that are more reactive for ET, while also reducing the frustration of the energy landscape, thus reducing the probability of the protein becoming energetically trapped in a less reactive conformation. These effects cannot be predicted from analysis of protein structure alone because there are no obvious electrostatic patches at the interface of the FMN and FAD domains in human CPR (Figure S5, Supporting Information). Thus, the exploration of energy landscapes requires the integration of solution biophysical spectroscopies (e.g., EPR/ELDOR) to identify multiple conformational states, with reactivity assays (e.g., stopped-flow measurements of ET) to establish the importance of the landscape to biological function.

Conclusions

ELDOR studies have identified multiple conformations of disemiquinoid CPR, consistent with there being a rugged energy landscape for domain motion in the enzyme. Functional studies have provided evidence for a gated conformational sampling mechanism for internal ET. The equilibrium distribution of conformational states can be perturbed through solvent (ionic strength and viscosity) and pressure perturbation and rationalized in terms of the known crystal structures of CPR that allude to the importance of multiple closed and open conformational states. Closed states are favored by nucleotide binding and favor internal ET, whereas more open states provide P450 enzymes access to electrons resident in the FMN-domain. This emphasizes the highly dynamic nature of biological ET embedded in conformational sampling mechanisms and the importance of ligand binding (and solvent properties) in poising the equilibrium across the functional energy landscape.

Acknowledgment. We thank the UK Biotechnology and Biological Sciences Research Council (N.S.S., Professorial Fellowship and project support) and TgK Ltd (S.B., studentship). N.S.S. is a Royal Society-Wolfson Merit Award holder.

Supporting Information Available: Additional EPR and kinetic data. This material is available free of charge via the Internet at http://pubs.acs.org.

JA1016206